PROGRESS IN COLOR, COLORANTS AND COATINGS

available online @ www.pccc.icrc.ac.ir

Progress in Color Colorants Coating 19 (2026), 23-36

Ministry of Science, Research and Technology
Institute for Color Science & Technology

Isotherm, Kinetic and Thermodynamic Investigation of Pb(II) Adsorption onto Magnetic Activated Carbon Fabric (MACF)

S. Kazemi Moghadam[1], F. Dadashian[*1], M. Montazer[1], M. Abedi[2]

[1.] Department of Textile Engineering, Amirkabir University of Technology, P.O. Box: 15875-4413, Tehran, Iran.

[2.] Department of Chemical Technologies, Iranian Research Organization for Science and Technology (IROST), P.O. Box: 33535-111, Tehran, Iran.

ARTICLE INFO

Article history:
Received: 15 Apr 2025
Final Revised: 07 July 2025
Accepted: 08 July 2025
Available online: 23 Sep 2025

Keywords:
Lead removal
Adsorption kinetics
Magnetic-activated carbon fabric
Adsorption isotherm
Thermodynamics

ABSTRACT

This study focuses on enhancing activated carbon fabric (ACF) designed for the adsorption of lead ions. Magnetic-activated carbon fabric (MACF) was produced from cotton fabric by a sonication technique and iron salt to improve its efficiency in Pb^{2+} adsorption from aqueous solutions. BET, XRD, SEM, FT-IR, and VSM analyses were applied to characterize MACF and ACF. The optimal conditions were pH = 4, an initial Pb^{2+} concentration of 50 mg/L, and an adsorbent dosage of 1.5 g/L, with the process conducted at 20±1 °C, 200 rpm for 1 hour for the removal of lead ions. Adsorption equilibrium data, including thermodynamics, isotherms, and kinetic studies, were analyzed. Among the various isotherm models, the Freundlich model provided the best fit for MACF adsorption of Pb^{2+}, with the highest regression value of 0.8477. MACF achieved an 84 % removal efficiency of Pb^{2+}, significantly outperforming ACF, which only achieved 4 %. The use of iron salts in the sonosynthesis process notably enhanced the ACF adsorbent, making MACF a cost-effective and high-performance substitute for conventional activated carbons. Its versatility in shaping, sizing, and ease of separation from environmental or filtration systems positions it as a superior solution for eliminating heavy and toxic metals from aqueous solutions. Prog. Color Colorants Coat. 19 (2026), 23-36© Institute for Color Science and Technology.

1. Introduction

Pollution of the environment has posed a serious worldwide health threat over the centuries, largely driven by industrial activities such as battery plates and equipment to produce sulfuric acid, the electroplating industry, cable covers, mining, and textiles. These industries release a variety of hazardous substances, including heavy metals, into the environment. Lead (Pb) is a toxic heavy metal that, once introduced into the body, tends to accumulate in the bloodstream and various organs, including the liver, intestine, brain, and skin [1]. Pb is not biodegradable, unlike organic contaminants, and persists indefinitely in the environmental system [2, 3]. In humans, lead exposure has been associated with functional impairments in the reproductive, hepatic, immunological, endocrine, and neurological systems, as well as gastrointestinal systems and chronic severe diseases [4]. The pollution of water or wastewater by Pb is a significant ecological concern that endangers human well-being through the environment. Therefore, it is crucial to develop more efficient techniques to remove Pb from such water and solutions to safeguard the ecosystem.

Activated carbon (AC) is created from various carbon sources, including waste cotton and agricultural residues, and is used as an adsorbent material for the

*Corresponding author: * dadashia@aut.ac.ir
https://doi.org/10.30509/pccc.2025.167528.1388

elimination of contaminants such as hazardous substances and heavy metals from water due to its excellent adsorption capability, extensive specific surface area, and durability. This material possesses an internal surface area ranging from roughly 500 to 3000 $m^2\ g^{-1}$, and is generally synthesized through a series of intricate, multi-step processes using carbon-rich organic precursors [5]. While activated carbon (AC) efficiently eliminates numerous pollutants such as dyes and toxic metals, its capacity for binding heavy metals like lead has certain constraints [6]. These encompass restricted adsorption capacity, elevated ash content, uneven distribution of micropores, and inadequate functional groups for purposeful adsorption [7, 8]. Altering the exterior structure of ACs through chemical treatments, such as in-situ sonosynthesis of magnetic nanoparticles on their surface, enhances their ability to accumulate Pb and other toxic metals.

The worldwide decline in the quality of water has prompted researchers to investigate nanoparticles, like iron oxide and silica, as novel adsorbents for the purification of wastewater/water [9]. These nanoparticles possess outstanding magnetic properties and high bio-compatibility, making them easy to separate using an external magnetic field. Additionally, their comparably cost–effective and reusability propose them as a suggested substance for improving adsorption efficiency once integrated with activated carbon [10, 11]. Numerous reports have demonstrated the efficacy and the adsorption capacity of AC for removing toxic material and metallic elements, particularly highlighting that their active sites serve a more pivotal function.

In this process [12, 13], activated carbon fibers (ACFs) are able to have some functional groups on their outer layer, thereby boosting their efficiency in adsorbing heavy and toxic metals [14]. In 2018, activated carbon fibers (ACFs) were first derived from waste cotton fabric and utilized as adsorbents for pollutant gases [15]. ACFs are considered suitable for diverse environmental and industrial applications due to their convenience in handling and effective elimination, which are crucial for effective adsorption and straightforward adsorbent management. To date, published studies concerning the application of modified activated carbon by nano-particles exhibit primarily concentrated on AC in powdered, granular, or fiber forms. We have developed and published, for the first time, the application of modified activated carbon fabric (MACF) enhanced with iron oxide nanoparticles to improve its adsorption capacity for removing heavy metals (Cu and Cd) from aqueous solutions [16].

An examination of the current literature on the application of ACF or its modified forms for extracting Pb from aqueous solutions highlighted a critical research gap. Iron oxide nanoparticles have arisen as promising substances for boosting adsorption potential after combining with ACF. They provide superior biocompatibility, magnetic properties, and easy removal. Due to the decreasing quality of wastewater/ water becoming a global concern, scientists are increasingly concentrating on iron oxide nanoparticles as great-performance adsorptive materials for wastewater/water purification and decontamination. Their reusability and cost-effectiveness make them an appealing option for enhancing adsorption efficiency. The synergistic combination of iron oxide nanoparticles and ACFs presents a promising solution to extract toxic and heavy metals from polluted wastewater/water [16, 17].

In this study, the objective was to examine the adsorption isotherms, kinetics, and thermodynamics of Pb^{2+} using MACFs. By analyzing these aspects, the research aimed to gain a more profound comprehension of how surface alterations impact the adsorption efficiency of MACFs for Pb^{2+}. These findings provide valuable insights into how these modifications influence the removal of Pb^{2+} from water/wastewater, potentially offering broader environmental benefits.

2. Experimental

2.1. Materials

Waste cotton fabric (170 g/m²) was sourced from Yazd Baft Co. (Iran). To ensure the use of high-purity reagents, all chemicals employed in this study, including hydrochloric acid (HCl, 37%), ortho-phosphoric acid (H_3PO_4, 85%), ferrous sulfate ($FeSO_4 \cdot 7H_2O$), sodium hydroxide (NaOH), lead (II) nitrate ($Pb(NO_3)_2 \cdot 4H_2O$), were completely obtained from Merck (Germany).

2.2. Materials synthesis

2.2.1. Preparation of activated carbon fabrics

Activated carbon fabric (ACF) was produced from discarded cotton fabrics through chemical reaction using H_3PO_4, as described previously [16]. Briefly, the optimal conditions for preparing ACFs involved an impregnation ratio of 2, a heating rate of 7.5 °C per minute, an activation temperature of 500 °C, and an

activation duration of 30 minutes. Post-synthesis, the ACFs were rinsed with distilled water to remove excess reagents until achieving a neutral pH of 7.

2.2.2. Preparation of magnetic-activated carbon fabric

Nanoparticles of iron oxide (Fe_3O_4) were synthesized on ACFs via sonosynthesis within a solution of $FeSO_4 \cdot 7H_2O$ (16 mM). The combination was subjected to ultrasonic treatment (37 kHz, 80W) at a pH of 10-11, adjusted gradually with 0.5 M NaOH, for 40 minutes at 75 °C. Afterward, the magnetic activated carbon fabrics were washed with distilled water and air-dried at 20°C (Figure 1, provided in the Appendix, illustrates the preparation procedure of magnetically activated carbon fabric (MACF).

2.2.3. Magnetic-activated carbon fabric in-situ synthesis

Magnetic activated carbon fabric was produced as previously outlined [16]. In summary, cotton fabric was treated with H_3PO_4 and then heated to 500 °C, converting the cellulose-based cotton into activated carbon. This transformation method introduces carboxyl (-COOH) and hydroxyl (-OH) groups on the surface of the ACF. When exposed to ultrasound in water, hydrogen peroxide (H_2O_2) and other radicals are produced. The carboxyl and hydroxyl groups on the activated carbon fabric are securely attached to Fe_3O_4 nanoparticles, forming a consistent structure, and are also physically trapped within its pores. This technique produces magnetite-activated carbon fabrics with improved applications.

2.3. Characterization methods

The BET surface area and pore volume of the nanoparticles were assessed by the BJH desorption method with nitrogen adsorption and desorption at 77 K, measured via a Quanta Chrome analyzer. The pH point of zero charge (pH_{pzc}) for activated carbon fibers (ACF) and magnetic activated carbon fibers (MACF) was determined using HCl and NaOH solutions, with pH levels adjusted between 2 and 12. After mixing the samples in these solutions, the pH was measured after 24 hours to determine the pH_{pzc} [18].

To analyze the samples, X-ray diffraction (XRD) was carried out via a Philips X-Ray diffractometer, and the average nanoparticle size was calculated with the Scherrer equation [19]. The surface morphology of ACF and MACF was examined using a Field Emission Scanning Electron Microscope (FESEM), and the elemental composition was determined using Energy-Dispersive X-ray Spectroscopy (EDX). Fourier-transform infrared (FT-IR) spectrometry was utilized to identify fabric characteristics, while a Vibrating Sample Magnetometer was used to measure the magnetic properties of MACF, applying a maximum magnetic field of 2 T at 20 °C.

2.4. Batch adsorption methods

The batch adsorption experiments were conducted to assess the removal of Pb^{2+} ions from solutions. Each trial involved preparing 50 mL of a Pb^{2+} ion solution at a specific concentration, with the initial pH set to 4. MACFs were introduced at a concentration of 1.5 g/L. Sealed tubes containing the solutions were maintained under agitation at a temperature of 20 ± 1 °C, using a rotary shaker (HLB501 Behsan, Iran) operating at 200 rpm; the MACFs were retrieved with forceps after agitation. The remaining concentration of Pb^{2+} ions in such solution was determined using Atomic Absorption Spectroscopy (PYE Unicam SP9 Atomic). Equation 1 was used to calculate metal removal percentages (R%) [20].

$$R\ (\%) = \frac{C_i - C_e}{C_i} \times 100 \quad (1)$$

Given (C_i) as the initial metal concentrations in the solution and (C_e) as the equilibrium metal concentrations in the solution, the adsorption capacity of MACF at equilibrium (q_e) was computed using the following equation (equation 2) [21].

$$q_e\ (mg/g) = \left[\frac{C_i - C_e}{M}\right] \times V \quad (2)$$

In equation 2, V shows the solution volume (L), and M represents the mass of MACF (g). The pH effect on the Pb^{2+} adsorption was studied by adjusting pH levels between 2 and 7. Adsorption isotherms were evaluated at several concentrations between 20 and 120 mg/L. For investigating kinetics, the contact time was varied from 20 to 90 minutes. Samples were collected at specific intervals, and the ion concentrations in each supernatant were measured using Atomic Absorption Spectroscopy (IR, PYE Unicam SP9 Atomic). Additionally, levels of Pb^{2+} before and after adsorption under optimal conditions were assessed using activated carbon fibers

(ACF) and magnetic activated carbon fibers (MACF), which were analyzed using inductively coupled plasma optical emission spectroscopy (ICP-OES, Varian 730-ES).

3. Results and Discussion

3.1. Characterization of MACF

The BET, XRD, SEM, FTIR and VSM results were determined for ACF and MACF, the MACF's specific surface area and overall pore volume are slightly less than those of ACF, decreasing from 633 ± 5 m^2/g and 0.16 ± 0.01 cm^3/g to 513 ± 4 m^2/g and 0.11 ± 0.01 cm^3/g for enhancing adsorption by introducing extra binding sites and enhancing their active surface area, which results from forming basic functional groups such as OH and COOH during the process of magnetic modification [16, 22].

The XRD (Figure 1) proved the amorphous structure of MACF with 22 % crystallinity and 12 to 17 nm crystal size of magnetic nanoparticles (23, 24). Diffraction peaks at 2θ angles of 30°, 35°, 42°, 53°, 56°, and 62° in MACFs indicate the presence of the magnetite phase, with no signs of hematite.

Scanning Electron Microscopy (SEM) images (Figure 2) show that the activation process maintains the original morphology of ACF (Figure 2a) and MACF (Figure 2b), with no noticeable structural alterations after modification. Iron oxide nanoparticles, roughly ranging in size from 60 to 120 nm (Figure 2c), are irregularly allocated across the MACF surface and show mild agglomeration.

The analysis of FT-IR results showed the existence of different functional groups on surfaces of ACF and MACF (Figure 3). In MACF, prominent absorption peaks at 544 and 784 cm^{-1} were observed, confirming the presence of iron oxide nanoparticles through their characteristic Fe-O and Fe-OOH stretching bands on the surface [25, 26]. At 1415 cm^{-1}, ACF displayed a peak suggestive of alkyl groups, including methyl and methylene. Peaks at 169 cm^{-1} in MACF and 1704 cm^{-1} in ACF indicated the existence of the carboxyl group (C=O). In MACF, peaks at 156 cm^{-1} and in ACF at 1587 cm^{-1} indicate aromatic structures. Moreover, MACF exhibited a pronounced -C-O band at 1216 cm^{-1}, pointing to a greater abundance of oxygen-containing functional groups [27].

Adsorbents possessing functional groups like aldehyde, ester, carboxyl, ketone, and hydroxyl are capable of binding heavy metal ions. The affinity for metal uptake is influenced by factors such as the number and accessibility of binding sites. In general, FT-IR analysis highlighted the impact of iron oxide, alkyl, aromatic groups, carboxyl, and hydroxyl groups over the surface of MACF for efficient adsorption of heavy metals. This enhanced ability is achieved through both complexation with physical adsorption mechanisms and functional groups [28], chemical reactions with surface sites, ion exchange, or surface precipitation [29].

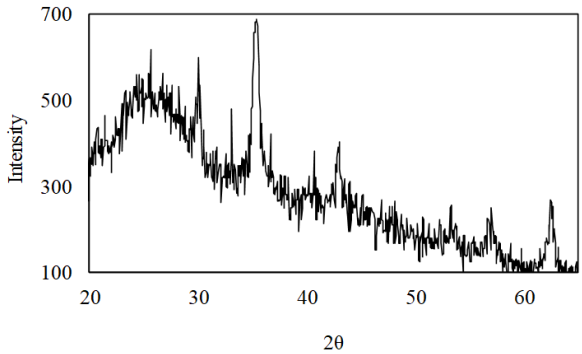

Figure 1: XRD graph of MACF.

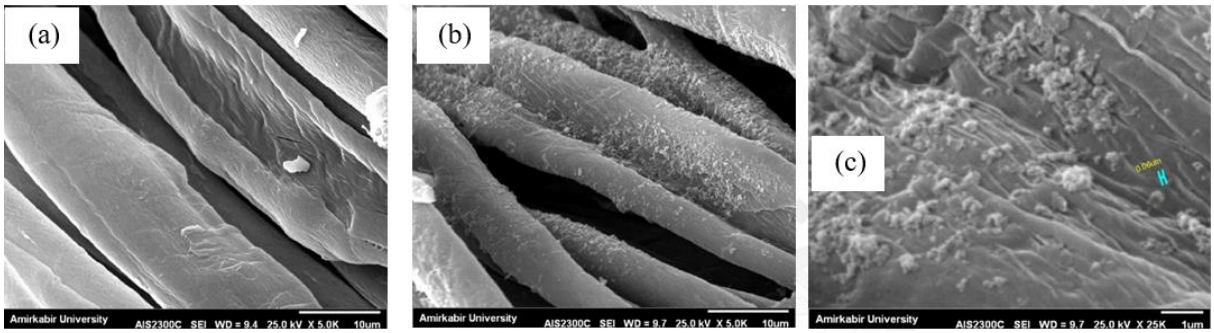

Figure 2: SEM micrographs of (a) ACFs with 5000X magnification, (b) MACFs with 5000X magnification, and (c) Nanoparticle size on the surface of MACF with 25000X magnification.

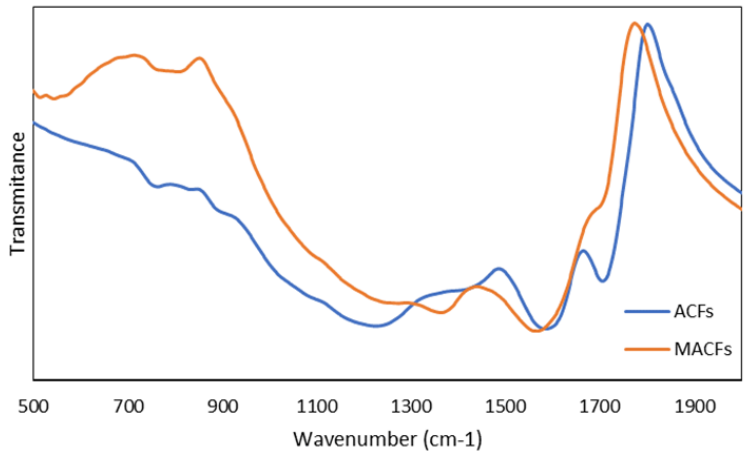

Figure 3: FT-IR spectra of ACFs and MACFs.

The VSM of MACFs demonstrated the saturation magnetization of 4.5 emu/g. Also, MACFs exhibit a definite value to external magnetic fields. This notable saturation magnetization allows MACFs to react to magnetic influences rapidly, enabling prompt separation from such solutions polluted by heavy or toxic metals. These observations are consistent with previous studies [30, 31].

3.2. Characterization of batch adsorption

3.2.1. Effect of solution pH on adsorption

To assess how chemical precipitation affects the elimination of Pb^{2+} ions, a control experiment was carried out without employing magnetic activated carbon fabric. The experiment demonstrated that Pb^{2+} removal does not occur at pH levels below 4. However, at pH levels above 4, Pb^{2+} ions start to precipitate as lead hydroxide ($Pb(OH)_2$), leading to complete removal from the solution at pH = 4.

Based on this finding, lead ion adsorption studies were carried out within a pH range of 2 to 7. The influence of pH on Pb^{2+} removal efficiency and adsorption capacity was examined using MACFs to identify the optimal adsorption pH. Other experimental conditions, including the concentration of lead ions (50 mg/L), MACF amount (1.5 g/L), speed of stirring (200 rpm), temperature (20 °C), and duration (1 h), were maintained at a constant level.

The study showed that the maximum Pb^{2+} removal efficiency and capacity occurred at pH = 4 (Figure 4). As the pH increased from 2 to 4, Pb^{2+} removal efficiency in the magnetic activated carbon fabric rose from 9.2 to 84 %. This improvement is attributed to functional groups like hydroxyl (-OH), carboxyl (-COOH), and ester ('RCOOR), as well as surface electrostatic charges that enhance ionic bonding. These observations align well with earlier results for copper and cadmium [16].

At lower pH levels, Pb^{2+} adsorption was reduced due to competition with hydronium ions for adsorption sites, leading to lower adsorption efficiency. In contrast, at higher pH levels, functional groups on the MACF deprotonate, creating negatively charged sites. This modification promotes electrostatic interactions with Pb^{2+} ions, leading to improved adsorption efficiency [30, 32].

Furthermore, the point of zero charge (pH_{pzc}) plays a critical role in assessing pH effects. The pH_{pzc} for the magnetic activated carbon fabric was determined to be 9.7. As a result, at pH = 2, the material undergoes enhanced electrostatic repulsion compared to pH = 4, leading to reduced adsorption efficiency at pH = 2 relative to pH = 4.

3.2.2. Effect of initial concentration of metal ions on adsorption

Figure 5 demonstrates how the initial concentration of Pb^{2+} ions affects their removal efficiency and capacity using magnetic activated carbon fabric, within a range of 25 to 200 mg/L (ppm), with other variables held constant. The results show that as Pb^{2+} ion concentration increases from 25 to 150 ppm, removal efficiency increases by 84.6 % and removal capacity reaches 127 mg/g. However, beyond 150 ppm, the efficiency drops to 64.3 % and the capacity remains constant as concentration increases to 200 ppm.

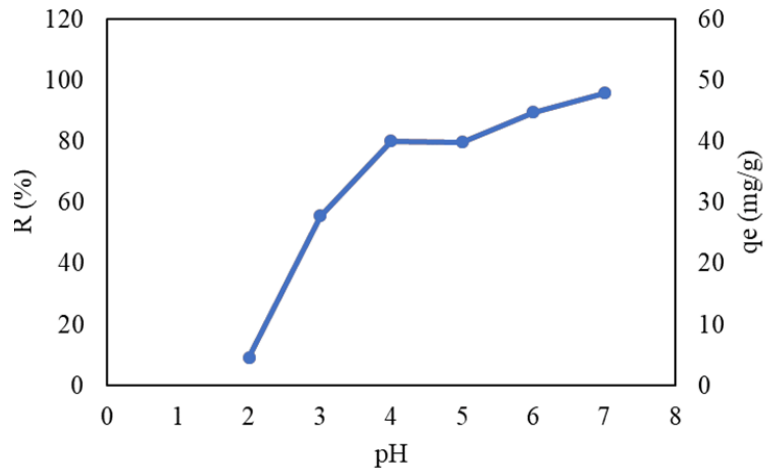

Figure 4: Impact of pH on Pb^{2+} adsorption efficiency and capacity of MACF.

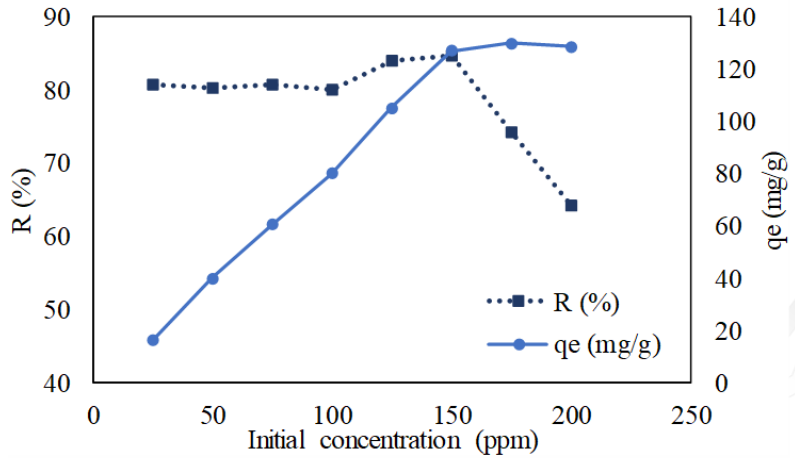

Figure 5: Effect of initial concentration on the removal of Pb^{2+} using MACF.

The decrease in efficiency at elevated concentrations stems from the saturation of accessible surface sites. As more metal ions populate these sites, the adsorption capacity of MACF diminishes, leaving fewer binding sites available. Consequently, removal efficiency declines. Therefore, a higher percentage of adsorption is observed at lower concentrations, where numerous active sites on the fabric surface are available [33].

The increase in adsorption capacity is primarily due to higher initial concentrations of metal ions, which enhance the diffusion of Pb^{2+} ions from the solution phase to the activated carbon fabric's surface. This heightened concentration strengthens the driving force for ion movement, leading to more interactions between lead ions and the magnetic nanoparticles within the fabric, boosting adsorption capacity [19]. However, once the concentration surpasses 150 ppm, adsorption sites become saturated, resulting in a decline in removal efficiency.

3.2.3. Influence of contact duration on adsorption

The study investigated the effect of contact time on the removal effectiveness and capacity of Pb^{2+} ions using MACFs, aiming to determine the optimal equilibrium duration (Figure 6). Experiments were conducted over a timeframe of 5 to 70 minutes, with other variables held constant. Findings indicated an increase in removal efficiency with longer contact times, achieving 96 % removal within the first 10 minutes as adsorption equilibrium was reached.

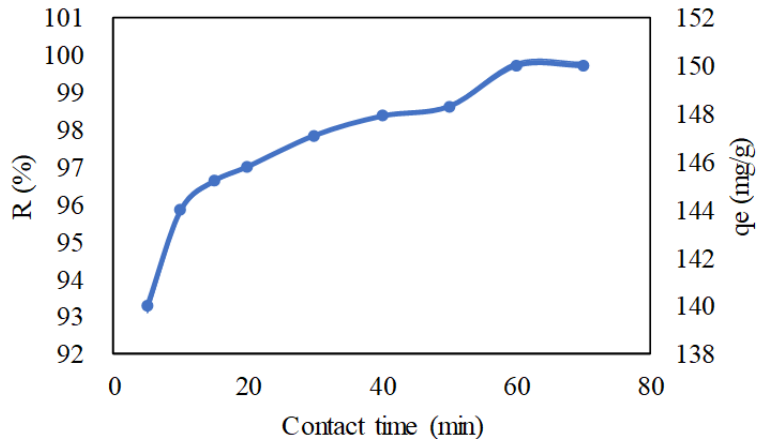

Figure 6: Influence of contact time on Pb^{2+} adsorption efficiency and capacity of MACF.

Despite equilibrium being quickly established, the experiments continued for a full 60 minutes to ensure complete ion adsorption. Initially, the removal rate was rapid due to the abundant surface area of the fabric, but it slowed down once equilibrium was reached, with the removal amount stabilizing. This pattern is attributed to the swift initial adsorption of lead ions onto the fabric.

After reaching equilibrium, the removal efficiency remained stable, as adsorption sites were fully occupied, limiting the fabric's capacity for additional ion adsorption. The adsorption trend of the magnetic fabric shows that lead ion adsorption peaks quickly with increased contact time and then stabilizes, which is similar to previous studies [32, 34].

3.2.4. Thermodynamics of adsorption

Thermodynamic analyses assist in identifying whether the adsorption procedure is physical or chemical. The thermodynamic parameters, specifically standard entropy (ΔS°), standard Gibbs free energy (ΔG°), and standard enthalpy (ΔH°), are involved in this determination. Equations 3 to 6 [35] were employed to calculate the removal of Pb^{2+} by MACF.

$$\Delta G° = -RT \ln K \quad (3)$$

$$\Delta H° = \left[\frac{RT_1T_2}{(T_2-T_1)}\right] \ln\left(\frac{K_2}{K_1}\right) \quad (4)$$

$$\Delta S° = \left(\frac{\Delta H° - \Delta G°}{T}\right) \quad (5)$$

$$K = \left(\frac{qe}{Ce}\right) \quad (6)$$

Where R (8.314 J mol^{-1} K^{-1}) represents the entire gas constant, K is the equilibrium constant specific to T, T K is the absolute temperature, Ce (mgL^{-1}) is the equilibrium concentration, and q_e is the total Pb^{2+} adsorbed on the MACF surface.

Studies of thermodynamics help in understanding the characteristics of the adsorption procedure and determining whether it is physical or chemical. The thermodynamic parameters, including standard entropy (ΔS°), standard Gibbs free energy (ΔG°), and standard enthalpy (ΔH°), were examined for the adsorption of Pb^{2+} ions on the surface of MACF.

Based on Table 1 data, a negative ΔG° value indicates that the adsorption process is spontaneous and feasible. This finding aligns with the Langmuir separation factor (RL) being between and 1, suggesting a favorable adsorption process. Similarly, the Freundlich exponent (n) is greater than 1, which also supports the favorable adsorption characteristics of lead ions onto MACFs.

The positive ΔH° value suggests that the adsorption process is endothermic, meaning it absorbs heat from its surroundings. This does not necessarily imply the process is irreversible, but reflects the energy changes during adsorption. Furthermore, the positive ΔS° value indicates increased disorder at the interface between the solid and solution. These changes in entropy, combined with the enthalpy value, affect Gibbs free energy and confirm the adsorbent surface's high affinity for Pb^{2+} ion adsorption.

Table 1: Thermodynamic parameters associated with the removal of Pb^{2+} by MACFs at 293 K.

ΔS° (J $mol^{-1}K^{-1}$)	ΔH° (J mol^{-1})	ΔG° (J mol^{-1})
33.5	6398.03	-3409.3

3.2.5. Adsorption isotherms

An evaluation of batch adsorption data has been conducted using various models, including the Freundlich and Langmuir models. The Langmuir model posits that an adsorbent possesses a specific number of uniform binding sites, each exhibiting identical affinity for adsorbing, making it applicable for characterizing monolayer adsorption on particular sites of the adsorbent material. According to this model, each adsorption site can accommodate just one molecule, forming a monolayer. The Langmuir model, along with the separation factor (R_L), is typically represented in its linear equation form as equations 7 and 8 [35].

$$q_e = \frac{Q_0 K_L C_e}{1+K_L C_e} \quad (7)$$

In equation 7, q_e (mg g^{-1}) represents the equilibrium adsorbate uptake per unit mass of adsorbent, Q_o (mg g^{-1}) denotes the maximum adsorption ability of the adsorbent, K_L (L mg^{-1}) is the Langmuir constant related to the adsorption energy, and Ce signifies the equilibrium concentration of the adsorbate (mgL^{-1}) [35].

The value R_L (equation 8) acts as an indicator of adsorption type: it indicates promosing adsorption when $R_L < 1$, linear adsorption when $R_L = 1$, unfavorable adsorption when $R_L > 1$, and irreversible adsorption when $R_L = 0$, with C_o representing the initial adsorbate concentration in milligrams per liter (mg/L).

$$R_L = \frac{1}{1+K_L C_0} \quad (8)$$

Langmuir adsorption factors Q_0 and K_L for Pb^{2+} ions have been calculated based on the intercept and slope of the Langmuir plot comparing C_e with C_e/q_e (Figure 7a). The maximum adsorption capacity (Q_0) for Pb^{2+} was found to be 200 mg g^{-1}, with a Langmuir constant (K_L) of 0.03. The R^2 value for Pb^{2+} adsorption using MACF in the Langmuir model was 0.80, indicating a moderate fit to the model. The R_L value for Pb^{2+} adsorption was determined to be 0.52, suggesting that the adsorption process for Pb^{2+} is moderately favorable.

In the Freundlich model, a linear plot of ln q_e versus ln C_e was used to determine the values of 1/n and ln K_F for Pb^{2+}, obtained from the slope and intercept, respectively (Figure 7b). The Freundlich exponent (n) for Pb^{2+} adsorption was found to be 1.33, and the K_F value was 7.80. The R^2 value for the Freundlich model was 0.85, higher than the R^2 value from the Langmuir model, indicating that the Freundlich model provided a better fit for Pb^{2+} adsorption onto MACF.

The Freundlich model, which accounts for adsorption on heterogeneous surfaces and suggests multilayer adsorption, indicates that Pb^{2+} adsorption onto MACF likely involves a multilayer process on a non-uniform surface. This contrasts with the monolayer adsorption described by the Langmuir model. The higher correlation of Pb^{2+} adsorption with the Freundlich model suggests that the adsorbent surface has varied affinities for Pb^{2+} ions, supporting the notion of a heterogeneous adsorption process [20].

3.2.6. Adsorption kinetics

Adsorption kinetics govern the rate and pathways of adsorption reactions, affected by the chemical and physical characteristics of the adsorbent. In the present study, three models were used to evaluate the adsorption kinetics: pseudo-first-order, pseudo-second-order, and intraparticle diffusion models. The pseudo-first-order kinetic model, according to the Lagergren equation (Eq. 10), was utilized to elucidate adsorption within the solid-liquid system [36]. This model assumes that each metal ion is bound to a single sorption site on the surface of the adsorbent.

$$\ln(q_e - q_t) = \ln q_e - k_1 t \quad (10)$$

Based on the pseudo-first-order model, q_e denotes the equilibrium uptake capacity, whereas q_t (mg g^{-1}) represents the adsorption capacity at a given time t (min). The adsorption rate constant K_1 (min^{-1}) is calculated from the linear plot's slope of ln(q_e-q_t) against time (min) (Figure 8a). For Pb^{2+}, Equilibrium values of q_e (mg g^{-1}), K_1 (min^{-1}), and the regression R^2 values were determined to be 9.36, 0.037, and 0.9522, respectively. Among the models tested, the pseudo-first-order model showed the weakest fit, as indicated by its lower R^2 values.

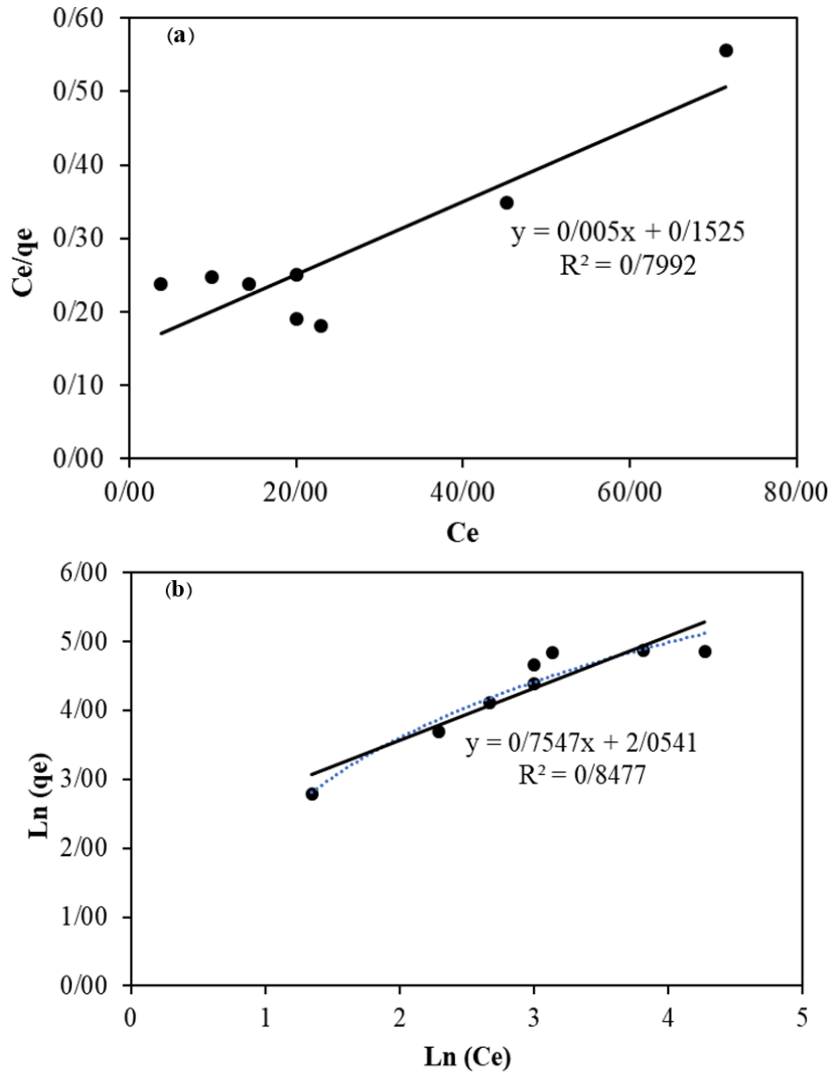

Figure 7: Adsorption isotherm of Pb^{2+} on MACF: (a) Langmuir and (b) Freundlich.

The pseudo-second-order model (equation 11) was applied to study Pb^{2+} adsorption by MACF (Figure 8b). This model assumes each metal ion associates with two distinct binding sites on the adsorbent surface, which is generally used for analyzing the kinetics of chemi-sorption from aqueous solution. within this framework, K_2 (g mg^{-1} min^{-1}) is the rate constant, while K_2 q_e^2 (mg g^{-1} min^{-1}) is the initial adsorption rate.for the pseudo-second-order model. From the slope and intercept of the linear t/q_t versus time (min) plot (Figure 8b), values for both $1/(K_2\ q_e^2)$ and $1/q_e$ are derived, facilitating the calculation of K_2 and q_e.

$$\frac{t}{q_t} = \frac{1}{k_2 q_e^2} + \frac{1}{q_e} t \qquad (11)$$

The values of K_2 (g mg^{-1} min^{-1}), q_e (mg g^{-1}), and R^2 for the adsorption of Pb^{2+} by MACF are 151.52, 0.012, and 0.99, respectively. The results indicate that the regression coefficients for Pb^{2+} are nearly 1, demonstrating a high degree of fit. Additionally, the experimental and calculated q_e values are very similar, indicating that the pseudo-second-order model provides a greater fit to the data compared to the pseudo-first-order model.

The Weber-Morris model (1963) is employed to evaluate the kinetic and diffusive properties of adsorption. This model (equation 12) delineates the transfer of ions from the solution to the solid phase, occurring in two distinct stages. Initially, in what is termed macropore diffusion, heavy metal ions migrate to the outer layer of MACF, a process referred to as external diffusion. The second stage, micropore diffusion, describes ion movement from the external surface into the internal MACF pores [37].

$$q_t = K_i t^{1/2} + I \qquad (12)$$

Weber-Morris model utilizes q_t (mg g^{-1}) as the binding capacity at time t (min), and determines the rate constant for intra-particle diffusion, K_i (mg g^{-1} $min^{-1/2}$), from the slope of the linear plot of q_t vs $t^{1/2}$ (Figure 8c). The intercept of this plot provides I, representing boundary layer thickness. In this study, K_i and I are 1.52 and 141.95, respectively. A higher I value indicates a significant boundary layer effect. If intra-particle diffusion were the sole mechanism, the plot would pass through the origin, but it does not, suggesting additional processes influence adsorption. Therefore, adsorption is not solely governed by intraparticle diffusion [38, 39].

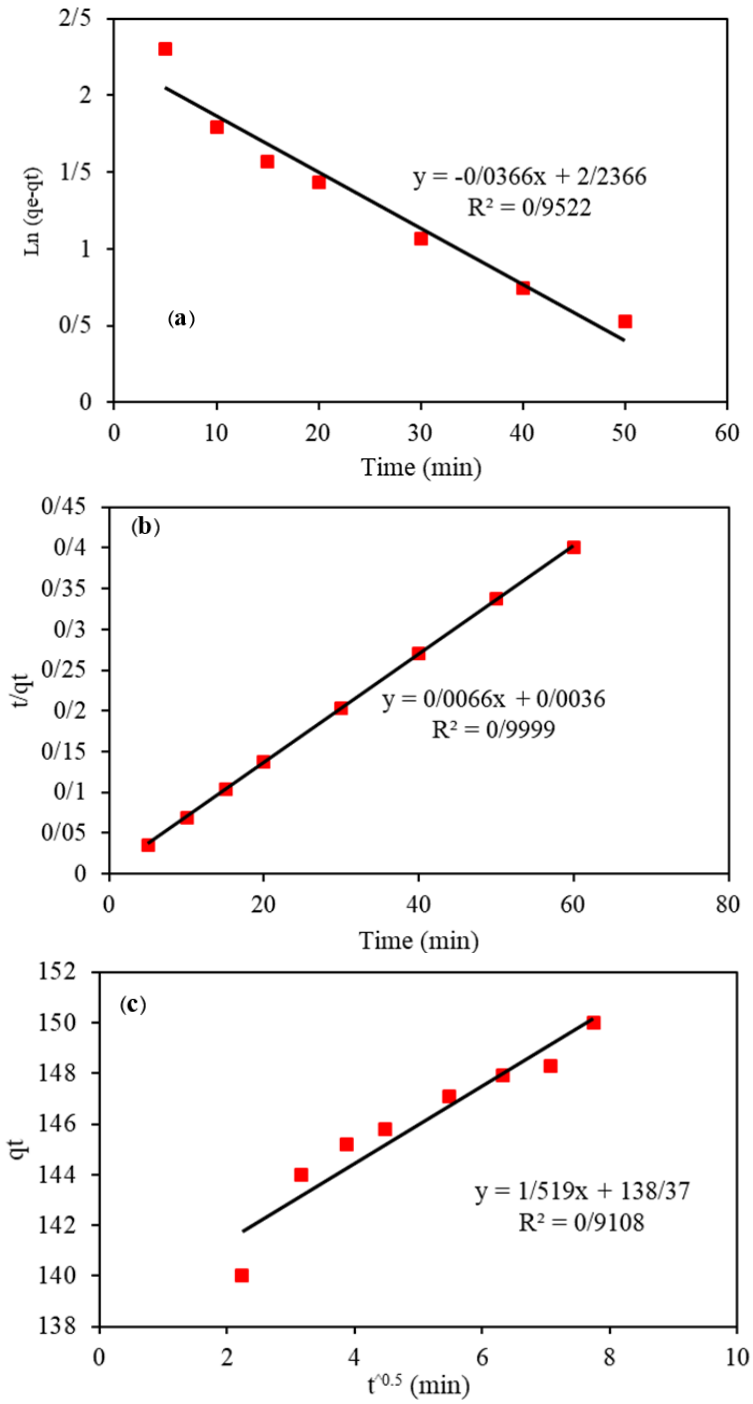

Figure 8: Kinetic models for the adsorption of lead by magnetic activated carbon fabric: (a) First-order model, (b) Second-order model, (c) Intra-particle diffusion model.

3.2.7. Comparing Pb^{2+} adsorption by MACF and ACF

The elimination of Pb^{2+} ions at varied initial concentrations with a pH level of 4 after 60 minutes was examined using both magnetic activated carbon fabric (MACF) and regular activated carbon fabric (ACF). The results show that the removal efficiency of Pb^{2+} by the magnetic fabric remains stable up to 150 ppm, but decreases beyond this concentration. Moreover, Pb^{2+} adsorption onto unmagnetized activated carbon fabric is significantly lower (R = 4 %). The adsorption capacity of ACF was enhanced through magnetic modification up to 84 % for Pb^{2+}, demonstrating the significant role of iron oxide nanoparticles in enhancing metal ion adsorption. These findings align with previous studies [27, 30, 34].

At pH values below pH_{pzc}, the surfaces of either ACF or MACF carry a positive charge, whereas at pH values over pH_{pzc}, a negative charge develops on their surfaces. At pH = 4, ACF, with a pH_{pzc} of 4.2, is expected to exhibit a higher affinity for metal ions due to greater electrostatic attraction in comparison to MACF, which has a pH_{pzc} of 7.9. However, results indicate that the presence of iron oxide nanoparticles significantly enhances the adsorption of Pb^{2+}. While iron oxide nanoparticles slightly reduce the pore volume and specific surface area, they significantly increase the number of functional groups and binding sites, thereby enhancing metal ion adsorption. Specifically, the surface of these nanoparticles is enriched with negatively charged functional groups, such as hydroxyl groups, which play a critical role in binding heavy metal ions through electrostatic interaction forces. These functional groups create active sites that facilitate strong interactions with positively charged heavy metal ions, such as Pb^{2+}, improving the overall adsorption efficiency [20].

Comparing this study with previous studies shows that Pb^{2+} adsorption by ACF is lower than for Cu^{2+} and Cd^{2+}, with its removal efficiency remaining below 10% [16]. Also, in MACF, Pb^{2+} removal efficiency is lower for Cu^{2+} and Cd^{2+}, with a decline in Pb^{2+} adsorption occurring beyond 150 ppm, whereas for Cu^{2+} and Cd^{2+}, this decrease is observed beyond 50 ppm.

This study, along with previous research [16], confirms that MACF is a highly efficient adsorbent for the removal of Pb^{2+} and other heavy metals from water. ACF can adsorb metals like copper, cadmium, and lead, but its modification with iron oxide nanoparticles significantly increases the adsorption capacity, allowing for the removal of larger amounts of contaminants. Although the addition of iron oxide may lead to a reduction in BET surface area, it increases binding sites and functional groups, improving performance [22]. The surface modification ensures strong attachment of nanoparticles to MACF, minimizing detachment. In cases of detachment, these biocompatible nanoparticles can be easily separated by a magnet. Iron oxide nanoparticles are fundamental in enhancing the adsorption efficiency of Pb^{2+} by MACF.

Table 2 presents a comparison of the adsorption capacity and efficiency of MACF with other activated carbon forms for Pb^{2+} removal, as reported in recent studies. The results demonstrate that MACF exhibits superior performance as an adsorbent for water purification, surpassing conventional activated carbon types. This enhanced efficiency is likely due to the incorporation of iron oxide nanoparticles and an increased presence of basic functional groups on the MACF surface. These findings are consistent with prior research indicating that granular activated carbon, post-chemical modification, typically offers higher adsorption capacities than powdered forms, primarily due to the enhanced formation of basic functional groups.

Table 2: Comparison of different studies.

Adsorbent	Source	Physical shape	Heavy metal	Adsorption capacity (mg g^{-1})	Removal (%)	References
AC/$FeCl_3$	Pistachio shell	Powder	Pb^{+}	112.36	94.5	[41]
AC	Rice husk	Powder	Pb^{+}	65	-	[42]
AC/Fe/clay	Coconut shell	Granule	Pb^{+}	74.2	-	[43]
AC/Fe	Commercial	Powder	Pb^{+}	-	86.87	[17]
ACF	Waste cotton	Fabric	Pb^{+}	1	4	This study
ACF/Fe	Waste cotton	Fabric	Pb^{2+}	127	84	This study

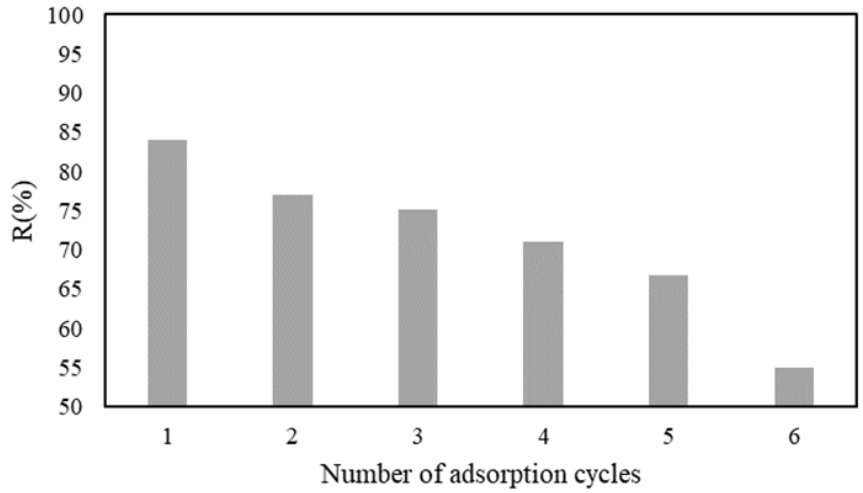

Figure 9: Adsorption cycle of Pb^{2+}using MACF from aqueous solution.

3.2.8. Lead ion Recovery

Figure 9 illustrates the adsorption efficiency of Pb^{2+} after being adsorbed by magnetic activated carbon fabric (MACF), followed by recovery and reuse of the magnetic fabric.

As illustrated in Figure 9, the efficiency loss for lead adsorption is primarily due to the strong affinity of Pb^{2+} ions to accumulate on the adsorbent surface, which makes detachment challenging. In the early cycles, the decrease in efficiency is minimal. However, after 6 cycles, the reduction becomes significantly more noticeable. Consequently, after six cycles, it is necessary to either replace the adsorbent or apply additional surface modifications to maintain its effectiveness [23].

4. Conclusion

In this study, Activated carbon fabric (ACF) magnetic with iron oxide nanoparticles (MACF)was used for the first time for Pb^{2+} ion removal. The results clearly showed that the adsorption performance of MACF was superior to that of ACF. The removal efficiency for Pb^{2+} remained consistently high at 84 % for concentrations up to 150 ppm. However, beyond this threshold, the efficiency significantly declined. This finding illustrates that sonosynthesis modification markedly improved heavy metal adsorption, due to the presence of iron oxide nanoparticles on the MACF surface. This study revealed that the Freundlich model more effectively characterized the adsorption process than the Langmuir model, indicating a heterogeneous surface and multilayer adsorption on MACF. Although the magnetic fabric exhibited a reduced BET surface area and iodine number, suggesting partial pore blockage by iron oxide nanoparticles, its exceptional adsorption performance highlights the pivotal role of these nanoparticles in enhancing metal ion removal.

Magnetically activated carbon fabric (MACF) emerges as a highly efficient and easily separable adsorbent for water and wastewater treatment. The surface modification with iron oxide nanoparticles not only significantly boosts adsorption efficiency but also securely stabilizes these nanoparticles, reducing the risk of detachment and release into the environment. Consequently, MACF represents a promising approach for Pb^{2+} removal, advancing water treatment technologies, and mitigating environmental contamination.

5. References

1. Ara A, Usmani JA. Lead toxicity: a review. Interdiscip toxicol. 2015; 8(2):55. https://doi.org/10.1515/intox-2015-0009.
2. Goren AY, Recepoglu YK, Karagunduz A, Khataee A, Yoon Y. A review of boron removal from aqueous solution using carbon-based materials: an assessment of health risks. Chemosphere. 2022; 293:133587. https://doi.org/10.1016/j.chemosphere.2022.133587.
3. Al-mahbashi NMY, Kutty S, Jagaba A, Al-nini A, Sholagberu AT, Aldhawi BN, Rathnayake U.

Sustainable sewage sludge biosorbent activated carbon for remediation of heavy metals: Optimization by response surface methodology. Case Stud Chem Environ Eng. 2023; 8:100437. https://doi.org/10. 1016 /j.cscee.2023.100437.

4. Liu Z, Zhang FS, Sasai R. Arsenate removal from water using Fe_3O_4-loaded activated carbon prepared from waste biomass. Chem Eng J. 2010;160(1):57-62. https://doi.org/10.22059/ije.2021.320878.1485.
5. Deshannavar U, Singa PK, Gaonkar D, Gayathri A, Patil A, Malade LV. Removal of acid violet 49 and acid red 88 dyes from aqueous solutions using advanced oxidation process. Mater Today: Proc. 2020; 24:1011-9. https://doi.org/10.1016/j.matpr.2020.04.414
6. Sultana M, Rownok MH, Sabrin M, Rahaman MH, Alam SN. A review on experimental chemically modified activated carbon to enhance dye and heavy metals adsorption. Clean Eng Technol. 2022; 6: 100382. https://doi.org/10.1016/j.clet.2021.100382.
7. Shahrashoub M, Bakhtiari S. The efficiency of activated carbon/magnetite nanoparticles composites in copper removal: Industrial waste recovery, green synthesis, characterization, and adsorption-desorption studies. Microporous Mesoporous Mater. 2021; 311: 110692. https://doi.org/10.1016/j.micromeso.2020. 110692.
8. He J, Li H, Yang W, Lu J, Lu Y, Liu T, Shi S. Experimental study on erosion mechanism and pore structure evolution of bituminous and anthracite coal under matrix acidification and its significance to coalbed methane recovery. Energy. 2023; 283:128485. https://doi.org/10.1016/j.energy.2023.128485.
9. Cheng J, Ma R, Shi D, Liu F, Zhang X. Rapid growth of magnetite nanoplates by ultrasonic irradiation at low temperature. Ultrason Sonochem. 2011;18(5):1038 -42. https://doi.org/10.1016/j.ultsonch.2010.12. 008.
10. Harifi T, Montazer M. In situ synthesis of iron oxide nanoparticles on polyester fabric utilizing color, magnetic, antibacterial and sono-Fenton catalytic properties. J Mater Chem B. 2014;2(3):272-82. https://doi.org/10.1039/C3TB21445A.
11. Rastgoo M, Montazer M, Malek RM, Harifi T, Rad MM. Ultrasound mediation for one-pot sonosynthesis and deposition of magnetite nanoparticles on cotton/polyester fabric as a novel magnetic, photocatalytic, sonocatalytic, antibacterial and antifungal textile. Ultrason Sonochem. 2016; 31:257-66. https://doi.org/10.1016/j.ultsonch.2016.01.008.
12. Mughni NFA, Zulkifle NF, Radzi RS, Hidayah N, Arifin FK, Zainol A, Yusop FFM. A comparative analysis of granule and powder activated carbon derived from date seeds. APS. 2024:63. https://doi. org/10.3390/environsciproc2021009036.
13. Radhi AA. Comparison of granulated and powdered activated carbon in the removal of organic matter from river water. Int Res J Adv Eng Sci. 2020; 5:191-7. http://irjaes.com/wp-content/uploads/2020/10/ IRJAES- V5N3P352Y20.pdf
14. .Salehi R, Dadashian F, Abedi M, Hasani B. Optimization of chemical activation of cotton fabrics for activated carbon fabrics production using response surface methodology. J Text Instit. 2018; 109 (12):1586-94. https://doi.org/10.1080/00405000. 2018. 1436235.
15. Salehi R, Dadashian F, Ekrami E. Acid dyes removal from textile wastewater using waste cotton activated carbon: Kinetic, isotherm, and thermodynamic studies. Prog Color Colorant Coat. 2018; 11(1):9-20. https://doi.org/10.30509/pccc.2018.75738
16. Moghadam SK, Dadashian F, Montazer M, Abedi M. Magnetic-activated carbon fabric for removal of copper and cadmium ions: kinetics and thermodynamics studies. Water Air Soil Poll. 2025; 236(3):179. https://doi.org/10.1007/s11270-025-07781-x.
17. Payandeh K, Ghasemi S. Investigation of kinetics and equilibrium of lead-absorbing process by magnetic activated carbon powder with Fe_3O_4 nanoparticles from aqueous solutions. J Water Wastewater. 2019; 30 (2). https://doi.org/10.22093/wwj.2018.117362. 2613.
18. Baassou Z, Benmahdi F, Reffas A, Benhaya A. The effect of impregnation ratio and surface modification on the characteristics and performance of activated carbon derived from Ficus carica leaves for Cr (VI) removal. Biomass Conv Bioref. 2024: 1-14. https://doi.org/10.1007/s13399-024-05432-5.
19. Zailan SN, Mahmed N, Juzaini NM, Norizan MN, Mohamad IS, Bouaissi A. Magnetite (Fe_3O_4)-activated carbon composite from ground coffee waste for the removal of copper ions (Cu^{2+}) from solution. Internat J Nanoelect Mater (IJNeaM). 2024; 17:147-53. https:// doi.org/10.58915/ijneam.v17iDecember.1618.
20. Zadeh KK, Jafari D. Activated carbon/alginate/Fe_3O_4 magnetic nanocomposite as a superior functional material for removal of lead from aqueous media. Biomass Conv Bioref. 2024; 14(16):19025-43. https://doi.org/10.1007/s13399-023-04040-z.
21. Jain M, Yadav M, Kohout T, Lahtinen M, Garg VK, Sillanpää M. Development of iron oxide/activated carbon nanoparticle composite for the removal of Cr (VI), Cu (II) and Cd (II) ions from aqueous solution. Water Res Industry. 2018; 20:54-74. https://doi. org/10.1016/j.wri.2018.10.001.
22. Karthik D, Baheti V, Militky J, Naeem MS, Tunakova V, Ali A. Activated carbon derived from carbonization of kevlar waste materials: a novel single stage method. Materials. 2021; 14(21):6433. https://doi.org/10.3390/ma14216433
23. Zulaicha A, Buhani B, Nuralita A, Setiajaya A. Synthesis activated carbon from shell of Elaeis guineensis Jacq and modified with magnetite (AC-Fe_3O_4) as adsorbent for waste metal ion Pb (II) in waters. AIP Conference Proceedings; 2024: AIP Publishing. https://doi.org/10.1063/5.0208360.
24. Takmil F, Esmaeili H, Mousavi SM, Hashemi SA. Nano-magnetically modified activated carbon prepared by oak shell for treatment of wastewater

containing fluoride ion. Adv Powder Technol. 2020; 31(8):3236-45. https://doi.org/10.1016/j.apt.2020. 06. 015.
25. Sultana M, Rownok MH, Sabrin M, Rahaman MH, Nur Alam SM. A review on experimental chemically modified activated carbon to enhance dye and heavy metals adsorption. Clean Eng Technol. 2022; 6:100382. https://doi.org/10.1016/j.clet.2021.100382.
26. Shen YF, Tang J, Nie ZH, Wang YD, Ren Y, Zuo L. Tailoring size and structural distortion of Fe3O4 nanoparticles for the purification of contaminated water. Bioresour Technol. 2009;100(18):4139-46. https://doi.org/10.1016/j.biortech.2009.04.004.
27. Iles A, Zaoui F, Daouadji BE, Zorgani MA, Siddig LA, Abdelhamid AS, et al. Removal of pollutants by olive stones-derived activated carbon@ Fe_3O_4 nano-composites: Effect of calcination temperature on adsorption properties. J Water Proc Eng. 2024; 66: 105960. https://doi.org/10.1016/j.jwpe.2024. 105960.
28. Alswat AA, Ashmali AM, Alqasmi TM, Alhassani HR, Alshorifi FT. Role of nanohybrid NiO–Fe_3O_4 in enhancing the adsorptive performance of activated carbon synthesized from Yemeni-Khat leave in removal of Pb (II) and Hg (II) from aquatic systems. Heliyon. 2023; 9(3). https://doi.org/10.1016/j.heliyon. 2023.e14301.
29. Dave PN, Chopda LV. Application of iron oxide nanomaterials for the removal of heavy metals. J Nanotechnol. 2014. https://doi.org/10.1155/2014/ 398569.
30. Abdulqader WH, Abbas JA. Oak tree leaves activated carbon with magnetite nanoparticles for the removal of Pb (II) ions from aqueous solutions. Iranian J Ichthyol. 2023; 10:219-37. https://www.ijichthyol.org /index.php/iji/article/view/954.
31. Nguyen MD, Tran H-V, Xu S, Lee TR. Fe_3O_4 nanoparticles: structures, synthesis, magnetic properties, surface functionalization, and emerging applications. Appl Sci. 2021;11(23):11301. https://doi. org/ 10.3390/app112311301.
32. Ali AA, Abdul-Hameed HM. Synthesis and characterization of magnetic activated carbon manufactured from palm stones by physical activation to remove lead from aqueous solution. Desalination Water Treatment. 2025; 321:100951. https://doi.org/ 10. 1016/j.dwt.2024.100951.
33. Wang B, Lan J, Bo C, Gong B, Ou J. Adsorption of heavy metal onto biomass-derived activated carbon. RSC Adv. 2023; 13(7):4275-302. https://doi.org/10. 1039/D2RA07911A.
34. Mahmoodi M, Aslibeiki B, Sakha MA, Zarei M. Oleaster seed-derived activated carbon/ferrite nano-composite for Pb^{2+} removal from wastewater. Mater Chem Phys. 2023; 300:127536. https://doi.org/10. 1016/ j.matchemphys.2023.127536.
35. Mohamed SMI, Yılmaz M, Güner EK, El Nemr A. Synthesis and characterization of iron oxide-commercial activated carbon nanocomposite for removal of hexavalent chromium (Cr^{6+}) ions and Mordant Violet 40 (MV40) dye. Sci Reports. 2024;14 (1): 1241.https://doi.org/10.1038/s41598-024-51587-6.
36. Mahmouda AS, Youssefa NA, Abo El Nagab AO, Selimc M. Removal of copper ions from wastewater using magnetite loaded on active carbon (AC) and oxidized active carbon (OAC) Support. J Sci Res Sci. 2019; 36(1):226-47. https://doi.org/ 10.21608/jsrs.2 019.34280.
37. Su Q, Zhang J, Wang X, Li Y, Lin S, Han J. Adsorption removal of copper (II) and chromium (VI) from wastewater by Fe_3O_4-loaded granular activated carbon. Water Practice Technol. 2024; 19(1):99-112. https://doi.org/10.2166/wpt.2023.220.
38. Liu Y, Chen M, Yongmei H. Study on the adsorption of Cu (II) by EDTA functionalized Fe_3O_4 magnetic nano-particles. Chem Eng J. 2013; 218:46-54. https://doi.org/10.1016/j.cej.2012.12.027.
39. Zhou XY, Zhou JL, Guo R, Liu Yj, Yu Yf, Zhang B, et al. Effect of flue gas components on the removal of cadmium pollutants by transition metal-modified activated carbon: Density functional theory and thermodynamic study. Fuel. 2023; 343:128011. https://doi.org/10.1016/j.fuel.2023.128011.

How to cite this article:
Kazemi Moghadam S, Dadashian F, Montazer M, Abedi M. Isotherm, Kinetic and Thermodynamic Investigation of Pb(II) Adsorption onto Magnetic Activated Carbon Fabric (MACF). Prog Color Colorants Coat. 2026;19(1):23-36. https://doi.org/10.30509/pccc.2025.167528.1388.